A method for measuring the geometrical topography of a Rockwell diamond indenter

2010 Meas. Sci. Technol. 21 015307

(http://iopscience.iop.org/0957-0233/21/1/015307)

Meas. Sci. Technol. **21** (2010) 015307 (7pp) doi:10.1088/0957-0233/21/1/015307

A method for measuring the geometrical topography of a Rockwell diamond indenter

Yen-Liang Chen[1,2] **and Der-Chin Su**[1]

[1] Department of Photonics and Institute of Electro-Optical Engineering, National Chiao-Tung University, 1001 Ta-Hsueh Road, Hsinchu 30050, Taiwan, Republic of China
[2] Center for Measurement Standards/Industrial Technology Research Institute (ITRI), Bldg 16, 321, Kuang Fu Rd, Sec. 2, Hsinchu 30031, Taiwan, Republic of China

E-mail: t7503@faculty.nctu.edu.tw (Der-Chin Su)

Received 21 July 2009, in final form 29 October 2009
Published 7 December 2009
Online at stacks.iop.org/MST/21/015307

Abstract
Firstly, a Rockwell diamond indenter tip is tested at different angles and positions by using a scanning white light interferometer, and several image data are obtained. Then, these data are merged together to form the associated geometrical topography with the image stitching method. Moreover, both the tip radius and the cone angle can be obtained with the least-squares Gauss–Newton sphere and cone fitting algorithm. Its validity is demonstrated.

Keywords: white light interferometer, image stitching method, Rockwell diamond indenter, surface topography, Mirau interferometer

1. Introduction

Because hardness is a key characteristic parameter of materials, the hardness measurement is a very important technique for characterizing the mechanical properties of materials [1]. A blunt conical Rockwell diamond indenter is often used to estimate the hardness of materials. The measured results strongly depend on the geometrical topography of the indenter [2–6]. It is necessary to identify the geometrical topography of the indenter in advance. Several pieces of apparatus [7–9] have been developed to measure the geometrical topography of the Rockwell diamond indenter with the contact stylus method. Although they have good results, they are time consuming for three-dimensional (3D) measurement. In 2004, Takagi *et al* [10] developed an interference microscope to measure the radius and the cone angle of a Rockwell diamond indenter tip quickly. But the radius is measured with the reflected light from the surface; it may have some errors if its surface deviates from an ideal spherical one. Besides, an accurate rotation device is needed for measuring the cone angle. To overcome those drawbacks, we present an alternative and convenient optical method with a two-dimensional white light interferometer [11–13] and the use of the image stitching method without an accurate rotation device. Because of the microscopic configuration of the two-dimensional white light interferometer, the measurable region is restricted and the overall topography cannot be obtained in a single measurement. It can be improved by measuring at different angles and positions. Several image data are obtained, and each set of data has a partial overlap with the neighboring one. Next, these data are merged together to form the associated topography with the image stitching method based on the iterative closest point (ICP) algorithm [14, 15]. In addition, two crucial parameters, the tip radius at the center and cone angle along the outside area of the overall 2D topography, can be calculated by using the least-squares Gauss–Newton sphere and cone fitting algorithm [16]. The validity of this method is demonstrated. It has some merits such as simple nondestructive measurement, wide measurement range, easy operation, rapid measurement and low cost.

2. Principle

2.1. Scanning white light interferometer

A Mirau-type scanning white light interferometer (SWLI) is used in this method and its configuration is shown in figure 1. It consists of a white light source WS, a

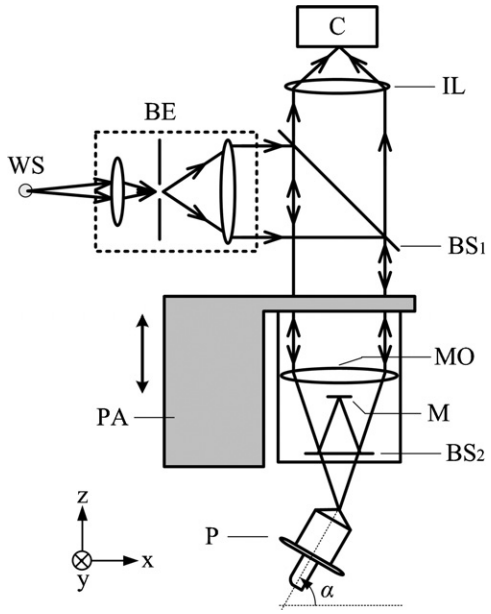

Figure 1. Schematic diagram of this method with a Mirau-type scanning white light interferometer. WS: white light source; BS: beam splitter; MO: microscopic objective; M: mirror; PA: precision actuator; P: microindenter tip; IL: imaging lens C: CCD camera.

beam-expander BE, a beam splitter BS_1, a Mirau-type microscopic objective located with a precision actuator PA, a Rockwell diamond indenter tip P, an imaging lens IL and a CCD camera C. Here the Mirau-type microscopic objective also has a beam splitter BS_2, a mirror M and a microscopic objective MO. The light beam coming from the WS is collimated by the BE. The collimated beam is reflected by the BS_1 and enters a Mirau-type microscopic objective, in which it is divided by the BS_2 into two parts: the reference beam and the test beam. They are focused on the M and the P, respectively; and both of them are reflected and come back along the original paths. Then, they pass through the BS_1 and the IL, and finally they enter the C. Hence, the interferogram recorded by the C can be approximated by a mean intensity $I_0(x, y)$ and a series of sinusoidal signals modulated by an envelope function as [17]

$$I(x, y, z) = I_0(x, y)\{1 + \gamma(x, y, z) \cdot \cos[\phi(x, y, z)]\}. \quad (1)$$

The envelope function $\gamma(x, y, z)$ is the fringe contrast, which varies much more slowly with the optical path difference (OPD) between two interfering beams than the phase difference $\phi(x, y, z)$. The basic principle of this method is that the maximum contrast occurs when the OPD is zero. The procedures for measuring the topography of the P are described as follows.

(1) Locate the P at a moderate azimuth angle and let the test beam be focused slightly higher than the P.
(2) Displace the PA step-by-step along the -z direction to vary the OPD and record the corresponding interferograms simultaneously by using the C. It is operated until the test beam is focused slightly lower than the P.
(3) Determine the positions of maximum contrast image points in every two-dimensional interferogram, and then record the data of their positions and the associated position of the PA in the z-axis.
(4) Combine the data recorded at different positions of the PA in procedure (3) together and the topography of the P can be obtained.
(5) Change the azimuth angle of the P and repeat the above procedures. Then, the associated topography of the P can be obtained similarly.

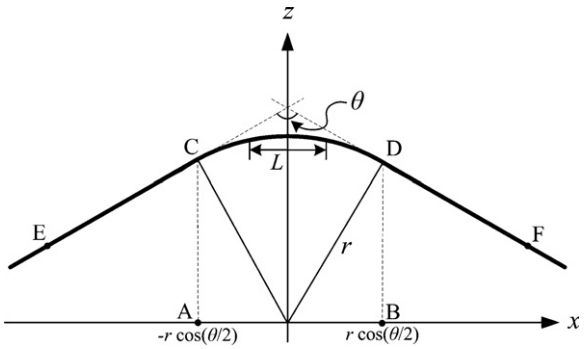

Figure 2. Geometrical relation of the tested blunt conical tip profile with $\alpha = 90^\circ$.

2.2. *Measurement criteria for a Rockwell diamond indenter*

A Rockwell diamond indenter with cone angle θ and tip radius of curvature r is shown in figure 2 with azimuth angle $\alpha = 90^\circ$ and it can be expressed as

$$z = \begin{cases} \left(|x| + r\sec\dfrac{\theta}{2}\right)\cot\dfrac{\theta}{2}, & \text{as } |x| \geqslant r\cos\dfrac{\theta}{2}, \\ \sqrt{r^2 - x^2}, & \text{as } |x| < r\cos\dfrac{\theta}{2}, \end{cases} \quad (2)$$

where $r > 0$ and $0 < \theta < \pi$. Its slope varies according to x as $|x| < r\cos\frac{\theta}{2}$ and it becomes a constant as $|x| \geqslant r\cos\frac{\theta}{2}$. The measurable solid angle depends on the numerical aperture NA of the MO and the associated slope of the tip. If the measurable range in a single test is L, then we have

$$\left|\left.\frac{dz}{dx}\right|_{x=\frac{L}{2}} - \left.\frac{dz}{dx}\right|_{x=-\frac{L}{2}}\right| \leqslant 2\tan\left(\frac{\sin^{-1}NA}{2}\right). \quad (3)$$

Equation (3) can be rewritten as

$$r \geqslant \frac{L}{2\sin\left(\frac{\sin^{-1}NA}{2}\right)}. \quad (4)$$

For easy measurement, the measured region should be kept horizontal. So, m measurements with different α by rotating the P around the y-axis, as shown in figure 3(a), should be operated to obtain the overall information. If the measurement range $|x| < r\cos\frac{\theta}{2} + L/2$ and the overlapping width $L/4$ of any two neighbor measurements are chosen, then we have

$$2r\cos\frac{\theta}{2} < (m-1)L - (m-1)\frac{L}{4} < r(\pi - \theta). \quad (5)$$

Here, m must be rounded up to an integer.

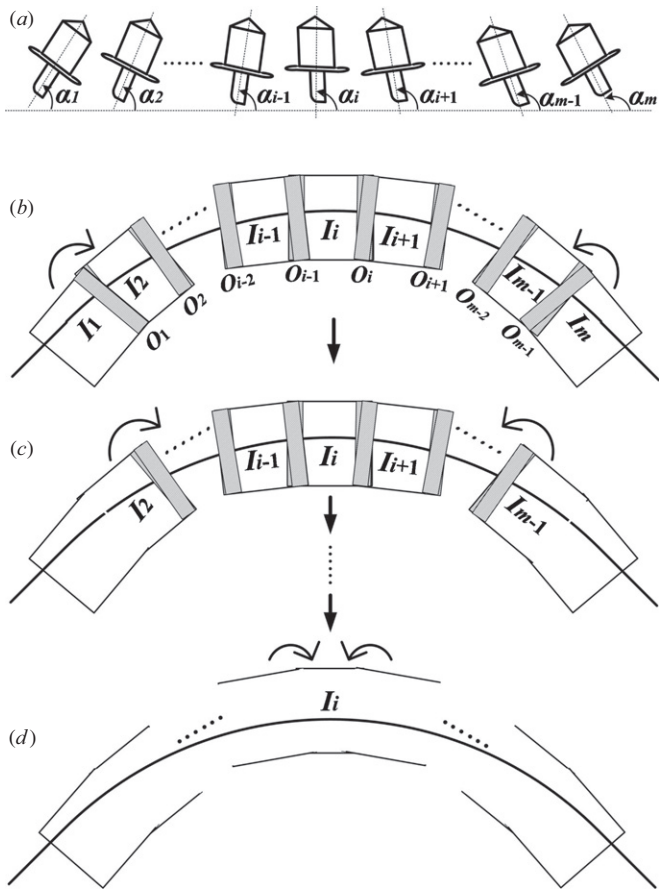

Figure 3. Image stitching procedures: (*a*) the tested tip at different α; (*b*) transformations of I_1 and I_m to the coordinate systems of I_2 and I_{m-1} via O_1 and O_{m-1}; (*c*) transformations of I_2 and I_{m-1} to the coordinate systems of I_3 and I_{m-2} via O_2 and O_{m-2}; (*d*) repeated transformations to the coordinate system of I_i and a stitched resultant image.

2.3. Image stitching for two adjacent images

The data in the overlapping regions of any two neighbor measurements need to be processed with the ICP algorithm [14, 15], and they become spatially matched to each other to be merged together. They are calculated in six degrees of freedom that include three rotations and three translations along the *x*-, *y*- and *z*-axes. For convenience, let the data of the overlapping regions of two adjacent images $F\{f_1, f_2, \ldots, f_k\}$ and $G\{g_1, g_2, \ldots, g_k\}$ be $OF\{of_1, of_2, \ldots, of_n\}$ and $OG\{og_1, og_2, \ldots, og_n\}$, respectively, so it is obvious that $OF \subset F$, $OG \subset G$, and every element is a 3×1 vector with (x, y, z) data. The procedures for transforming the data of F to the coordinate system of G and to be merged into G are described as follows.

(1) Transform the data of OF and OG with respect to their centroids [14]: the centroids are $of_c = (1/n)\sum_{i=1}^{n} of_i$ and $og_c = (1/n)\sum_{i=1}^{n} og_i$, respectively; of_c and og_c are 3×1 vectors. So, the associated data of $OF\{of_1, of_2, \ldots, of_n\}$ and $OG\{og_1, og_2, \ldots, og_n\}$ to their centroids are changed to $OA\{oa_1, oa_2, \ldots, oa_n\}$ and $OB\{ob_1, ob_2, \ldots, ob_n\}$, where $oa_i = of_i - of_c$ and $ob_i = og_i - og_c$.

(2) Derive the unit eigenvector: if the superscript T represents the transpose of a matrix, then the cross-covariance matrix $K = (1/n)\sum_{i=1}^{n} oa_i \cdot ob_i^{\mathrm{T}}$ can be obtained and K is also a 3×3 matrix. Let $K - K^{\mathrm{T}} = A(a_{ij})$ and $\Delta = [a_{23}\ a_{31}\ a_{12}]^{\mathrm{T}}$; then we have

$$Q(K) = \begin{bmatrix} \mathrm{tr}(K) & \Delta^{\mathrm{T}} \\ \Delta & K + K^{\mathrm{T}} - \mathrm{tr}(K) \cdot I_{(3\times 3)} \end{bmatrix}, \tag{6}$$

where $I_{(3\times3)}$ is the 3×3 identity matrix and tr( ) means the trace of a square matrix. Consequently, $Q(K)$ is a 4×4 matrix and its unit eigenvector is $q = [q_0 \quad q_1 \quad q_2 \quad q_3]$.

(3) Merge together: let

$$R_1 = \begin{bmatrix} q_0^2 + q_1^2 - q_2^2 - q_3^2 & 2(q_1q_2 - q_0q_3) & 2(q_1q_3 + q_0q_2) \\ 2(q_1q_2 + q_0q_3) & q_0^2 + q_2^2 - q_1^2 - q_3^2 & 2(q_2q_3 - q_0q_1) \\ 2(q_1q_3 - q_0q_2) & 2(q_2q_3 + q_0q_1) & q_0^2 + q_3^2 - q_1^2 - q_2^2 \end{bmatrix} \tag{7}$$

$$\tau_1 = og_c - R_1 \cdot of_c. \tag{8}$$

Then the intermediate data $O_1\{o_{11}, o_{12}, \ldots, o_{1n}\}$ can be obtained, where $o_{1i} = R_1 \cdot of_i + \tau_1$, R_1 is a 3×3 matrix; both τ_1 and o_{1i} are 3×1 vectors, respectively. If any element of τ_1 is larger than the setting threshold Δd, then $OF\{of_1, of_2, \ldots, of_n\}$ is replaced by $O_1\{o_{11}, o_{12}, \ldots, o_{1n}\}$. Next, the above procedures are operated repeatedly t times until all the elements of τ_t are smaller than Δd. Here, $R = R_1 \cdot R_2 \cdot \ldots \cdot R_t$ and $\tau = \tau_1 + \tau_2 + \cdots + \tau_t$ are the rotation matrix and the translation matrix, respectively. Finally, the data $\overline{F}\left\{\overline{f}_1, \overline{f}_2, \ldots, \overline{f}_k\right\}$, which transformed the data of F to G's coordinate system, are obtained, where $\overline{f}_j = R \cdot f_j + \tau$, and $j = 1, 2, \ldots, k$. The element $\overline{f}_j$ is a 3×1 vector with (x, y, z) data. Hence, the data of F and G have been merged together to the G's coordinate system.

2.4. Image stitching for multiple images

In the test, there are m images $(I_1, I_2, \ldots, I_m)$ with different α and $m - 1$ overlapping regions $(O_1, O_2, \ldots, O_{m1})$, as shown in figures 3(*a*) and (*b*). For convenience, the coordinate system of I_i is chosen as a reference coordinate and other images should be transformed to it. Here i may be $m/2$ or $(m + 1)/2$. Images I_1 and I_m are firstly transformed to the coordinate systems of I_2 and I_{m-1} via the associated overlapping regions O_1 and O_{m-1} respectively with the above procedures, as shown in figures 3(*b*) and (*c*). Then, the new merging images I_2 and I_{m-1} are also transformed to the coordinate systems of I_3 and I_{m-2} via O_2 and O_{m-2}, respectively, as shown in figure 3(*c*). These procedures are operated repeatedly until all the images are merged into one image, as shown in figure 3(*d*).

3. Experiments and results

A 50× Mirau objective lens (Nikon) with $NA = 0.55$ was used to test a Rockwell diamond indenter (Kinik Company) with specifications of 200 μm ± 20 μm tip radius and 120° ± 0.5° cone angle. The condition $m = 4$ was chosen according to

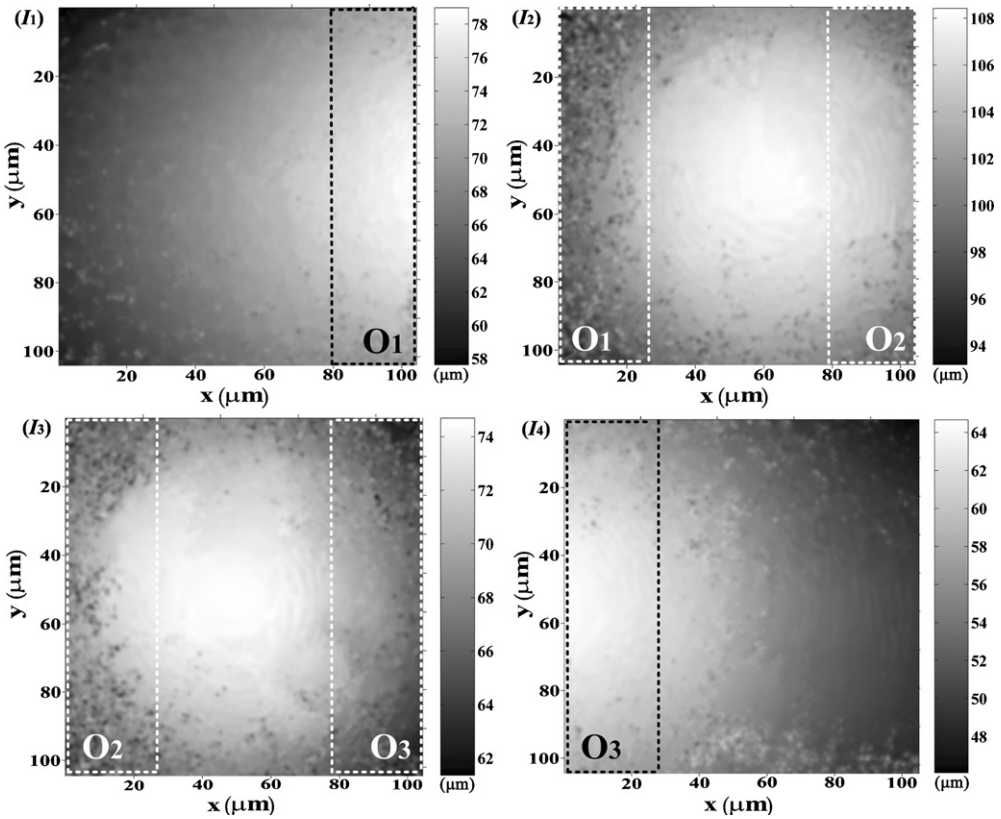

Figure 4. Four measured image data with three overlapping regions.

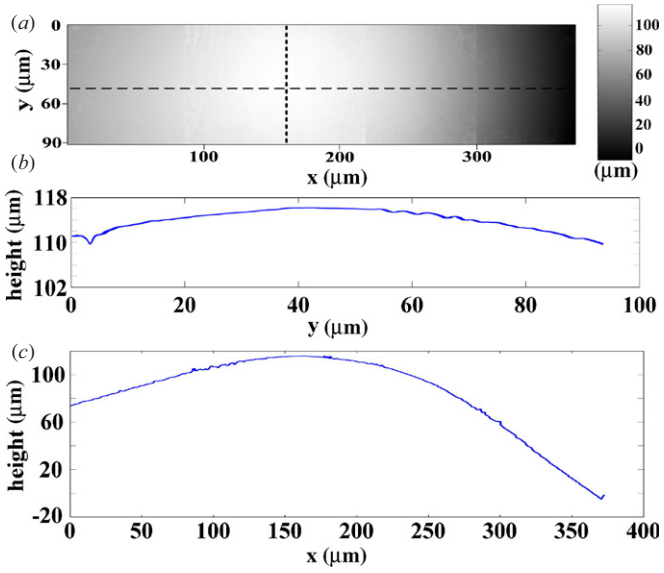

Figure 5. The measured results: (*a*) the resultant 2D topography in gray level and the profiles of (*b*) the dotted line and (*c*) the dashed line.

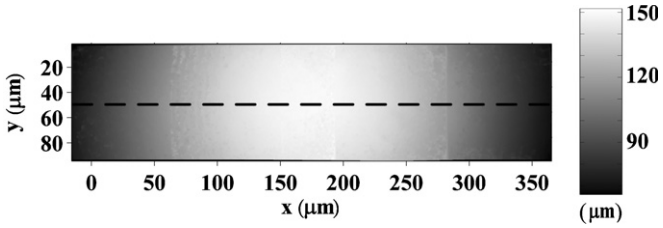

Figure 6. The orientated results of figure 5(*a*) for indenter geometry characterization.

equation (5) and they were operated at $\alpha \approx 70^\circ$, 80°, 100° and 110°. To compensate the brightness differences arising from different α, the intensity of the WS is so adjusted that good quality images can be taken. Their results are shown in figure 4 in gray level, which represents the corresponding relative height. Each image is recorded with 480×480 pixels and its dimension is $L \times L$, where $L = 104.2$ μm. These four image data were merged together with the conditions $\Delta d = 0.01$ μm and $i = 2$. The 2D topography with 1716×425 pixels was obtained and shown in figure 5(*a*). The cross profiles of the dotted line and the dashed line in figure 5(*a*) are calculated and depicted in figures 5(*b*) and (*c*), respectively. In addition, the tip radius and the cone angle can be estimated with the least-squares Gauss–Newton sphere and cone fitting algorithm [16] and they are 198.2 μm and 119.6°, respectively. The roundness value of the tip region is 4.3 μm.

For indenter geometry characterization, the stitching results in figure 5(*a*) are orientated onto the specifications given in the normative document [18] and they become the results as shown in figure 6. The data of the dotted line in figure 6 can be applied to depict the profile through the apex of the indenter tip. This profile was also measured by a commercial contact stylus instrument (ET4100, Kosaka Lab. Ltd). These two results are shown together in figure 7(*a*) for comparison; the solid curve and the dotted curve represent

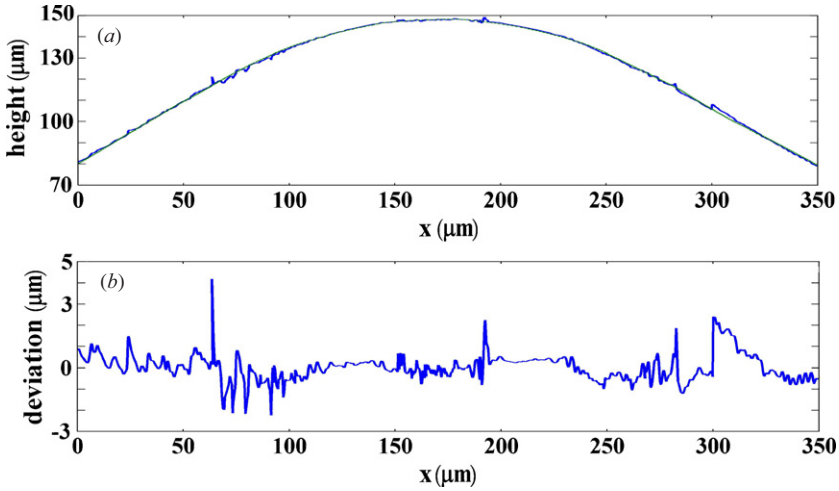

Figure 7. (*a*) Measured profiles through the apex of the indenter tip with this method (solid curve) and the contact stylus instrument (dotted curve); (*b*) their deviations.

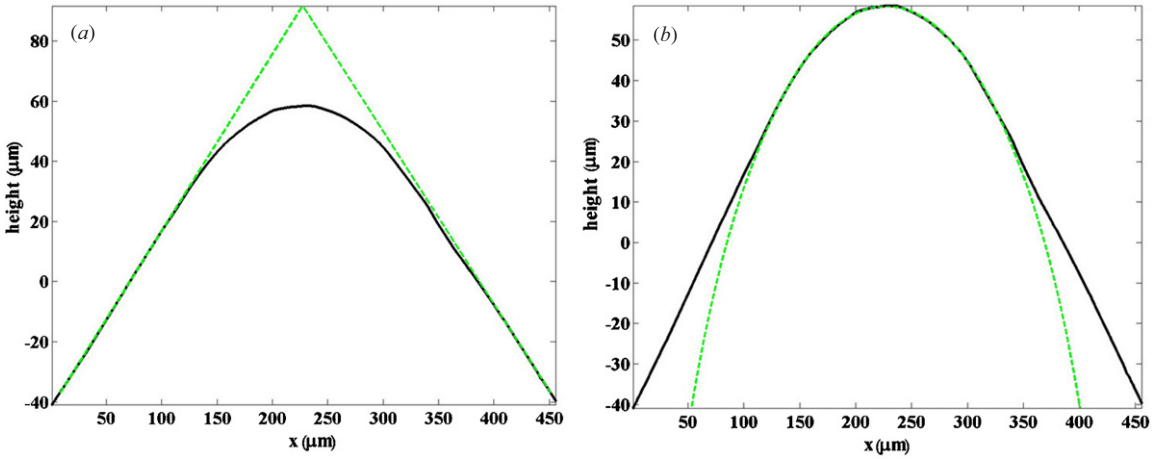

Figure 8. Geometries for calculating (*a*) the cone angle and (*b*) the tip radius of the P by using the least-squares fitting method with a stylus profiler.

the results of this method and the contact stylus instrument, respectively. Their deviations are shown in figure 7(*b*) and the cross correlation function [19] is up to 99.96%. Moreover, the measured results of the contact stylus instrument are also processed with the least-squares fitting algorithm; the curves for calculating the cone angle and the tip radius can be depicted as shown in figures 8(*a*) and (*b*), respectively. From these two curves, we can calculate their cone angle and tip radius to be 119.62° and 198.37 μm, respectively. It can be seen that both results are very consistent. According to ISO 6508-2 [18], the specifications for the shape of Rockwell indenters should be fixed as 200 μm $\pm$ 5 μm tip radius and 120° $\pm$ 0.1° cone angle. Based on these two measured results, we infer that the tested indenter may not be suitable for hardness calibration.

The area function [9] of the P is measured with this method, and the measured data (represented by dots) are depicted with the theoretical data (represented by a solid line) of an ideal Rockwell indenter in figure 9(*a*). Their radius deviations are plotted in figure 9(*b*) and the deviations vary abruptly at the border region between the ball cap and the cone frustum as Dai's results [9]. Because the maximum deviation is less than 2.5 μm, it is still less than the radius deviation tolerance 5 μm listed in ISO 6508-3 [20].

4. Discussion

The image stitching method is operated in full six degrees of freedom [14] to minimize the mean square distance and compensate the angle error between two sets of matched points. Although the P is tested at different α, a commonly used rotation holder ($\pm 1^\circ$) can be applied for tilting the indenter. The measured results in figure 4 are not in the same projection plane; however, the image features are similar in the overlapping region and two images can be matched very well to the nearest local minimum of a mean square distance. Because the data of I_1, I_3 and I_4 are rotated with respect to the y-axis to map the data of I_2 in the image stitching process, the data of stitched result will expand in the z-axis.

From equation (4), we can understand that the tip radius should be larger than 181 μm under our experimental

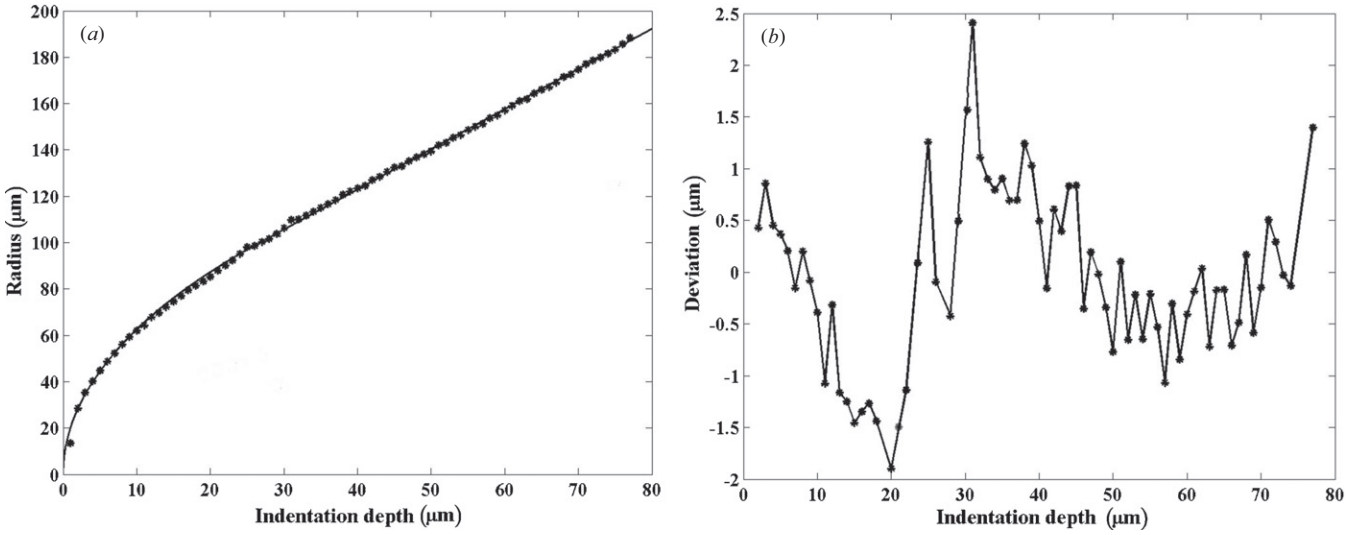

Figure 9. (*a*) The area function of the P is depicted with the measured data (represented by dots) and the theoretical data (represented by a solid line); (*b*) their deviations.

conditions. Consequently, this method is suitable for measuring a Rockwell diamond indenter tip. The measurement resolution of these four results in figure 4 can be discussed as follows.

(1) *Vertical measurement resolution.* It depends on the scanning linearity of the PA. The PA with a closed-loop circuit is used in our tests and it has 0.15% linearity. So, the measurement resolution in our tests is $\Delta z = 120 \times 0.15\% = 0.18\ \mu$m.

(2) *Lateral measurement resolution.* It depends on the diffraction limit of the microscopic system [21], and it can be expressed as

$$\Delta x = \Delta y \approx 0.61 \frac{\lambda_w}{NA} \approx 0.64\ \mu\text{m}, \tag{9}$$

where the central wavelength of the white light $\lambda_w \approx 580$ nm.

For simplicity, a Rockwell diamond indenter tip is set as figure 2 where $\alpha = 90^\circ$. Let the center of the sphere curvature be (0, 0, 0); then r is given as

$$r = \sqrt{x^2 + y^2 + z^2}. \tag{10}$$

The resolution of r can be written as

$$\begin{aligned}\Delta r &= \left|\frac{\partial r}{\partial x}\right| \cdot \Delta x + \left|\frac{\partial r}{\partial y}\right| \cdot \Delta y + \left|\frac{\partial r}{\partial z}\right| \cdot \Delta z \\ &= \frac{1}{r}(|x| \cdot \Delta x + |y| \cdot \Delta y + |z| \cdot \Delta z).\end{aligned} \tag{11}$$

Substitute Δx, Δy and Δz into equation (11); then we have a best resolution $\Delta r = 0.18\ \mu$m at $(x, y, z) = (0, 0, r)$. θ can be determined by lines $\overline{\text{CE}}$ and $\overline{\text{DF}}$ in figure 2, and their equations can be derived with the data of I_1 and I_4. They can be expressed as $z_1 = m_1 x_1 + k_1$ and $z_2 = m_2 x_2 + k_2$, respectively. Then we have

$$\theta = \pi - \tan^{-1}\left|\frac{x_1}{z_1}\right| - \tan^{-1}\left|\frac{x_2}{z_2}\right|. \tag{12}$$

Consequently, the resolution of θ is derived and written as

$$\begin{aligned}\Delta\theta &= 2 \cdot \left|\frac{\partial\theta}{\partial x_1}\right| \cdot \Delta x + 2 \cdot \left|\frac{\partial\theta}{\partial z_1}\right| \cdot \Delta z \\ &= \frac{2}{x_1^2 + z_1^2}(|z_1| \cdot \Delta x + |x_1| \cdot \Delta z).\end{aligned} \tag{13}$$

Substituting Δx and Δz into equation (13), the best resolution of cone angle can be evaluated as $\Delta\theta = 0.2^\circ$ where $(x_1, z_1) \approx (L, 0)$.

5. Conclusion

In this paper, an alternative method for determining the tip topography of the Rockwell diamond indenter has been proposed by introducing the imaging stitching method into a scanning white light interferometer. Four image data at different angles and positions have been obtained with a scanning white light interferometer. Each result should have a partial overlap with the neighboring one for image stitching. Next, these data have been merged to form the associated topography with the image stitching method based on the iterative closest point (ICP) algorithm. Moreover, two crucial parameters, the tip radius at the center and cone angle along the outside area of the overall 2D topography, have been calculated by using the least-squares Gauss–Newton sphere and cone fitting algorithm. The validity of this method has been demonstrated. It has some merits such as nondestructive measurement, wide measurement range, easy operation, rapid measurement and low cost.

Acknowledgment

This study was supported in part by the National Science Council, Taiwan, ROC, under contract NSC95-2221-E009-236-MY3.

References

[1] Tabor D 1970 The hardness of solids *Rev. Phys. Technol.* **1** 145–79

[2] Ma Q and Clarke D R 1995 Size dependent hardness for silver single crystal *J. Mater. Res.* **10** 853–63

[3] Swadener J G, George E P and Pharr G M 2002 The correlation of the indentation size effect measured with indenter of various shapes *J. Mech. Phys. Solids* **50** 681–94

[4] Wei Y and Hutchinson J W 2003 Hardness trends in micron scale indentation *J. Mech. Phys. Solids* **51** 2037–56

[5] Musil J, Zeman H, Kunc F and Vlcek J 2003 Measurement of hardness of superhard films by microindenter *Mater. Sci. Eng.* A **340** 281–5

[6] Zhang F, Huang Y and Hwang K C 2006 The indenter tip radius effect in micro- and nanoindentation hardness experiments *Acta Mech. Sin.* **22** 1–8

[7] Barbato G and Desogus S 1988 Measurement of the spherical tip of Rockwell indenters *J. Test. Eval.* **16** 369–74

[8] Song J F, Rudder F F, Vorburger T V and Smith J H 1995 Microform calibration uncertainties of Rockwell diamond indenters *J. Res. Natl Inst. Stand. Technol.* **100** 543–61

[9] Dai G, Herrmann K and Menelao F 2009 Two approaches for enhancing the accuracy of the Rockwell hardness test *Meas. Sci. Technol.* **20** 065701

[10] Takagi S, Ishida H, Usuda T, Kawachi H and Hanaki K 2004 Direct verification and calibration of Rockwell diamond cone indenters *HARDMEKO 2004* pp 149–54

[11] Kino G S and Chim S S C 1990 Mirau correlation microscope *Appl. Opt.* **29** 3775–83

[12] Deck L and Groot P 1994 High-speed non-contact profiler based on scanning white light interferometry *Appl. Opt.* **33** 7334–8

[13] Wyant J C 2002 White light interferoetry *Proc. SPIE* **4737** 98–107

[14] Besl P J and McKay N D 1992 A method for registration of 3D shapes *IEEE Trans. Pattern Anal. Mach. Intell.* **14** 239–56

[15] Pulli K 1999 Multiview registration for large data sets *Proc. Int. Conf. 3D Digital Imaging and Modeling* pp 160–8

[16] Shakarji C M 1998 Least-squares fitting algorithms of the NIST algorithm testing system *J. Res. Natl Inst. Stand. Technol.* **103** 633–41

[17] Sandoz P and Tribillon G 1993 Profilometry by zero order interference fringe identification *J. Mod. Opt.* **40** 1691–700

[18] ISO 6508-2 2005 Metallic materials—Rockwell hardness test: part 2. Verification and calibration of testing machines (scales A, B, C, D, E, F, G, H, K, N, T)

[19] Song J, Vorburger T, Renegar T, Rhee H, Zheng A, Ma L, Libert J, Ballou S, Bachrach B and Bogart K 2006 Correlation of topography measurements of NIST SRM 2460 standard bullets by four techniques *Meas. Sci. Technol.* **17** 500–3

[20] ISO 6508-3 2005 Metallic materials—Rockwell hardness test: part 3. Calibration of reference blocks

[21] Saleh B E A and Teich M C 1991 *Fundamentals of Photonics* (New York: Wiley)